NANO LETTERS

Letter

pubs.acs.org/NanoLett

Coupling of NV Centers to Photonic Crystal Nanobeams in Diamond

B. J. M. Hausmann,[†,⊥] B. J. Shields,[‡,⊥] Q. Quan,[†] Y. Chu,[‡] N. P. de Leon,[‡,∥] R. Evans,[‡] M. J. Burek,[†] A. S. Zibrov,[‡] M. Markham,[§] D. J. Twitchen,[§] H. Park,[‡,∥] M. D. Lukin,[‡] and M. Lončar*[,†]

[†]School of Engineering and Applied Sciences and [‡]Department of Physics, Harvard University, Cambridge, Massachusetts 02138, United States

[§]Element Six Ltd., King's Ride Park, Ascot SL5 8BP, United Kingdom

[∥]Department of Chemistry and Chemical Biology, Harvard University, 12 Oxford Street, Cambridge, Massachusetts 02138, United States

ABSTRACT: The realization of efficient optical interfaces for solid-state atom-like systems is an important problem in quantum science with potential applications in quantum communications and quantum information processing. We describe and demonstrate a technique for coupling single nitrogen vacancy (NV) centers to suspended diamond photonic crystal cavities with quality factors up to 6000. Specifically, we present an enhancement of the NV center's zero-phonon line fluorescence by a factor of ∼7 in low-temperature measurements.

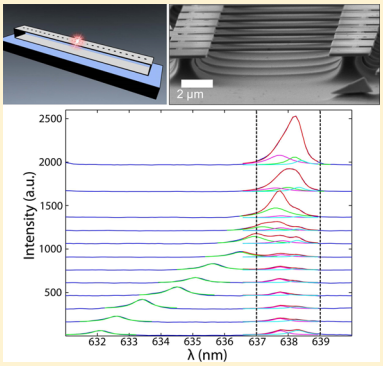

KEYWORDS: *NV center, diamond photonics, photonic crystal cavity, photonic crystal nanobeam*

The integration of solid state quantum emitters with subwavelength-scale optical devices has generated substantial interest in chip-based quantum networks.[1] Diamond is a particularly appealing platform for quantum photonics, as it is host to a number of different color centers[2] that can be individually integrated via ion implantation. Among them, the negatively charged NV center is an exceptional candidate for a quantum bit due to its spin readout and manipulation capabilities, which combined with long coherence times can be leveraged for quantum information science,[3−6] quantum sensing,[7−9] and quantum networks.[10,11] These potential applications all either require or benefit from optimized collection efficiency as well as control of spectral and spatial properties of spontaneously emitted photons.

An appealing approach to addressing these problems involves the use of cavity quantum electrodynamics (CQED). Here, the single photon spontaneous emission rate can be controlled by a photonic cavity that enhances the interaction strength between a single optical mode and the NV center. In the case of the NV center, these benefits can be realized by cavity coupling to the narrow-band zero-phonon line (ZPL) transition, which constitutes 3−5% of photoluminescent emission (PLE) from the excited state. Indeed, many applications in quantum science rely on the interference between indistinguishable photons for which only the ZPL transition is suitable. Coupling to an optical cavity thus provides a means to enhance both the ZPL collection efficiency and the relative proportion of photons emitted into the ZPL. In particular, photonic crystal cavities (PCCs), schematically depicted in Figure 1a, provide a strong enhancement due to their small mode volumes and have been studied widely in the context of light-matter interactions with quantum dots.[12,13]

To date, coupling between NV centers and PCCs has been demonstrated in several different systems that can be divided in two main categories: (i) hybrid and (ii) monolithic all-diamond approaches. Hybrid systems typically consist of cavities fabricated in nondiamond materials and are evanescently coupled to NV centers hosted in diamond nanocrystals. Examples include 2D PCCs cavities fabricated in GaP[14−16] and one-dimensional (1D) plasmonic PCCs based on silver nanowires.[17] On the other hand, monolithic, all-diamond approaches are based on optical cavities fabricated directly in single crystal diamond substrates. Examples include microring resonators,[18,19] 2D PCCs,[20] and 1D PCCs.[21,22] While hybrid approaches can be straightforward to implement, they suffer from inferior quality of NV centers found in diamond nanocrystals so far, as well as reduced overlap between cavity field and NV dipole. In this work, we demonstrate monolithic 1D PCCs fabricated from high purity single crystal diamond films with quality factors (Q) as high as 6000. We also demonstrate control of the cavity resonance using the combination of oxidation and diamond etching as well as inert-gas (Xe) deposition at low temperatures. Specifically, red tuning of the cavity resonance (up to 7 nm) using Xe

Received: June 15, 2013
Revised: October 15, 2013
Published: October 24, 2013

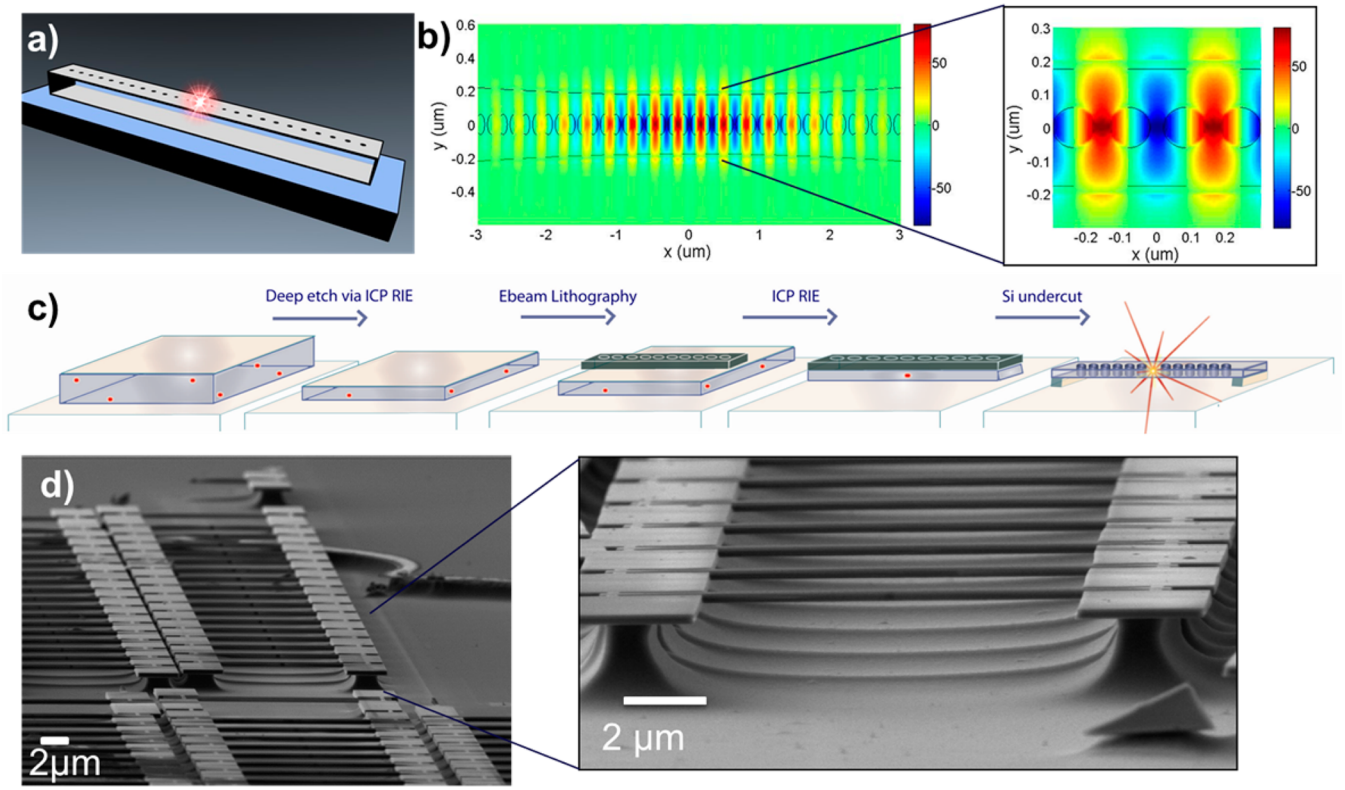

Figure 1. (a) Cartoon of a 1D photonic crystal nanobeam with an emitter coupled to the cavity. (b) FDTD modeling of the mode profile of a 1D photonic nanobeam. The hole diameter was constant while the width of the beam was tapered. (c) Fabrication schematic of diamond nanobeams: (i) a diamond membrane was thinned to the optical device layer in a deep reactive ion etch; (ii) next, EBL was performed to define the mask, and (iii) the mask was transferred into the diamond via RIE. (iv) Finally, the diamond nanobeams were undercut in an isotropic RIE step that removes the underlying Si layer. (d) SEM image of freestanding diamond nanobeams.

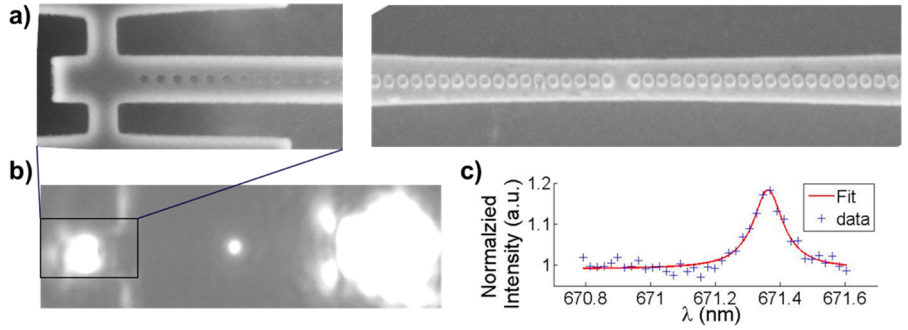

Figure 2. (a) SEM top view of a suspended photonic crystal nanobeam, (right) as well as of the outcoupling region for transmission measurements (left). (b) Transmission measurement obtained using white light from a supercontinuum source in-coupled at the right-hand side of the waveguide. Out-coupled and up-scattered light is observed both at the cavity region as well as the other end of the cavity. The scattering of the cavity mode is well localized, indicating tight light localization in the small mode-volume optical cavity. (c) Spectra obtained at the cavity region in transmission show cavity modes with Q factors up to ~6000.

deposition, and blue tuning of up to 23 nm was achieved by postfabrication diamond etching. Using these techniques we were able to bring the NV center in resonance with the cavity modes and demonstrate enhancement of the ZPL emission by a factor of 7 at low temperature.

To fabricate photonic crystals from a bulk piece of diamond, we employ a recently developed method for nanostructuring diamond.[18−20] As depicted schematically in Figure 1c, we begin with a type IIa, ⟨100⟩ crystal-oriented CVD or Ib HPHT single crystal diamond membrane (Element Six) of 20 μm thickness resting on a Si substrate. Next, we apply a deep reactive ion etch (RIE) in an oxygen inductively coupled plasma (ICP) to thin the membrane down to the desired device thickness of ~250 nm. We then define an etch mask via e-beam lithography (EBL) on a hydrogen silsesquioxane (HSQ, Krayden) resist film spun on the diamond substrate. A second oxygen RIE step transfers the mask pattern into the diamond thin film. Finally, we remove the substrate material from beneath the devices with an isotropic etch recipe for Si in a RIE, resulting in suspended nanobeams. Figure 1d shows a scanning electron microscope (SEM) image of several photonic crystal nanobeams (left) as well as a magnified view (right).

Modeling of 1D nanobeams was performed using the 3D finite difference time domain (FDTD) software Lumerical. Our

dx.doi.org/10.1021/nl402174g | Nano Lett. 2013, 13, 5791−5796

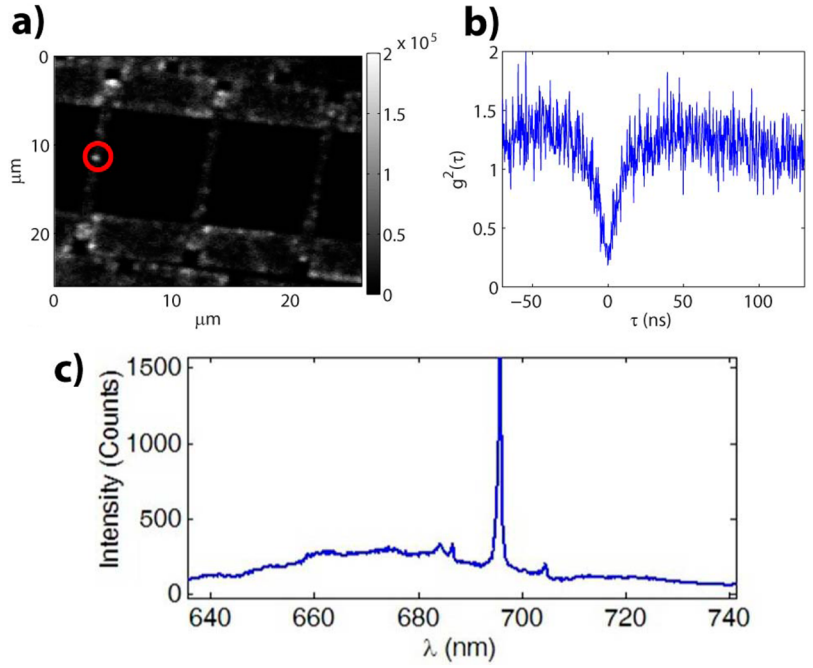

Figure 3. (a) Confocal microscope image of fluorescence from a device under excitation with 532 nm light. Individual NV centers are visible as bright spots along the nanobeam. (b) Second-order autocorrelation measurement of the fluorescence from an NV center in the cavity region of the nanobeam. The value for zero delay, $g^2(0) = 0.2$ is below 0.5, identifying it as a single NV center. (c) Fluorescence spectrum of the device collected directly from the NV center location. The broad phonon sideband of the NV center is coupled to the cavity at the resonance wavelengths (685, 695, 705, and potentially 682 nm) and the enhanced emission into the cavity is subsequently scattered into free space and collected by the objective along with the NV center emission.

photonic crystals consist of a series of holes etched through a diamond ridge waveguide, illustrated schematically in Figure 1a. Light is confined to the waveguide by the index contrast between diamond ($n = 2.4$) and air, while the periodicity of the holes forms a bandgap to confine light along the waveguide. The ability to store light in the cavity region in the time domain can be quantified by the Q factor. The particular parameters of our design were chosen to accommodate the inaccuracies of our fabrication process. In particular, devices obtained from the above procedure exhibit significant thickness variations from device to device across a single chip, owing to an initial thickness gradient in the mechanically polished diamond membrane, which is transferred to the film in the deep RIE step. As a result, we designed our photonic crystals to be robust to moderate variations in thickness within the range of 200–400 nm. To accomplish this, we used a relatively large hole radius (65 nm) and periodicity (ranging from 165 nm to 175 nm), which were kept uniform across the entire photonic crystal. The cavity is then formed by tapering the width of the waveguide down from 500 nm at the ends to 400 nm at the cavity center in a parabolic profile.[23,24] Coupling between the nanobeam photonic crystal cavity and an optical waveguide can be easily achieved[25] by modifying the geometry of the mirror holes at the ends of the photonic crystal. This allows for integration of multiple devices on the same chip and realization of integrated quantum networks. To achieve a high transmission signal ($T \propto Q_r^2/Q_{wg}^2$), the scattering Q factor ($Q \approx 8 \times 10^6$) was designed much larger than the waveguide Q. The waveguide limited ($Q \approx 5.3 \times 10^5$), total Q factor was determined to reach values up to $Q \approx 5 \times 10^5$ with a mode volume of $1.8 \times (\lambda/n)^3$, concentrated in the diamond (Figure 1b). Photons coupled into the optical waveguides were outcoupled at the end facet of the waveguide and collected using a lens with large numerical aperture (Figure 2a (left)).

In addition, we explore an alternative cavity design with a central hole removed. This cavity geometry features a moderate, scattering limited Q factor ($Q_{scattering} = 1 \times 10^4 < Q_{waveguide}$), mode volume of 3.7 $(\lambda/n)^3$ and multimode behavior but in turn increases the likelihood of locating an NV center in the cavity center. A top-view of a suspended nanobeam showing the width taper and filled in hole is presented in Figure 2a (right).

Characterization of the cavity spectral properties is performed in two ways. First, we probe the cavity response to a broadband input in a transmission configuration. We excite waveguide modes of the diamond nanobeam by coupling white light from a supercontinuum source (NKT Photonics) into the waveguide at one end. Light that is resonant will then couple to the cavity mode and, depending on the cavity design, either be scattered out from the cavity or transmitted to the far end of the waveguide and then outcoupled at the waveguide end. The balance between these two processes is determined by the ratio of scattering to waveguide-coupling Q factor. Figure 2b illustrates this behavior, with light focused onto the right end of the device and scattered from a well-localized spot at the cavity center and from the outcoupler at the left end of the waveguide. We collect the scattered light from each location and analyze its spectrum to obtain the cavity resonance frequency and Q factor (Figure 2c). With this method, we measured spectrometer-limited Q factors exceeding 6,000.

For devices containing an NV center, the cavity spectral properties can also be measured in the PLE spectrum of the NV center, as follows. The presence of an NV center in the vicinity of the cavity is determined by confocal microscopy. A 532 nm laser (Coherent Compass 315M) is focused onto the sample

dx.doi.org/10.1021/nl402174g | Nano Lett. 2013, 13, 5791–5796

and scanned over the field of view to excite randomly positioned NV centers defined during the growth of the diamond. Photons emitted from an NV center are then collected (green light is filtered out) and NV centers are identified as bright spots (Figure 3a). The presence of single NV centers was established by measuring the second-order autocorrelation of the PLE signal due to their characteristic antibunching dip (Figure 3b).[26] The (overall, non-filtered) NV PLE contains components from both charge states (NV^- and NV^0) and away from the ZPL provides a relatively flat, broadband source with which to probe the frequency of cavity modes over a range from ~575 to 800 nm. The emission of the NV center coupled to the cavity thus exhibits intensity peaks at the cavity resonances on top of a broad fluorescent background (Figure 3c). This approach can also be used to infer both the cavity frequency and Q factor, and these values were found to be in good agreement with values obtained using the white light transmission measurements. To further study our NV-cavity model system, we investigated the effects that the cavity has on the ZPL emission of the NV.

Integration of our cavities with NV centers for quantum optical applications requires spectral overlap with a narrow-band transition, associated with the ZPL. However, as discussed above, fabrication imperfections and diamond film wedging result in shifts of the cavity resonances from the predicted values, such that the cavity mode is, in general, not at the frequency of the ZPL transition. We employ two methods to tune our cavities, by either etching away material to blue-tune,[21] or condensing Xe gas to red-tune.[27] The two techniques are complementary with the etching method working well for coarse, unidirectional tuning over a large range (up to ~23 nm), while the red-tuning method can tune in finer, reversible, steps but over a shorter range (~7 nm). To take full advantage of these techniques we design our cavities to have the resonances positioned to the red of the ZPL. An etching approach is then used to blue-tune cavities toward the ZPL and bring their resonances within tuning range of the Xe condensation technique. The latter is then used to achieve precise, in situ, tuning of the cavity and to bring it in resonance with the ZPL frequency.

The blue-tuning was achieved using the following two etching methods: (i) an oxygen plasma etcher (Technics, Model 220) and (ii) a rapid thermal annealing in oxygen environment (Modular Process Technology, RTP-600xp). The effect of these techniques on the positions of a cavity resonance was studied over a series of etch steps of varying step lengths on a number of different cavities. The representative results are summarized in Figure 4 for a cavity with modest Q factor of ~1100. As can be seen, by varying the duration of the etch, we were able to tune the resonance in steps ranging from 0.2 to 5.3 nm. We also note that the plasma etching approach has more reproducible etch rates than the oxidation approach. In total, we were able to tune by ~23 nm over the course of eight etch steps without deterioration of the Q factor.

Once the cavity resonance was brought in the vicinity of the NV ZPL, as confirmed with the room-temperature measurements, the cavities were placed in a helium flow cryostat (Janis, ST-500) and cooled down to 4 K. The spectrum of a representative device is shown as the bottom trace in Figure 5a (zoom in to the ZPL shown in Figure 5b). It can be seen that the emission spectrum features five distinct peaks: the 573 nm peak corresponds to the diamond Raman line, the ~613, ~622, and ~631 nm peaks correspond to three cavity resonances,

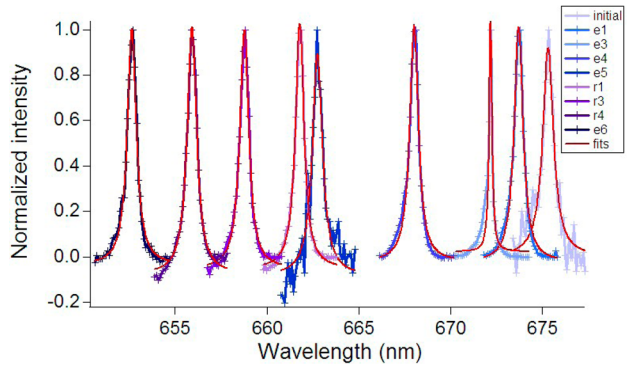

Figure 4. Controlled blue-tuning of a cavity mode via oxygen etching shown over eight etching steps. "e" refers to etching in an oxygen plasma etcher, while "r" refers to etch steps performed by annealing the samples in oxygen atmosphere in a rapid thermal processor. The etch times are of differing lengths, background has been subtracted, and modes are normalized by the peak intensity. An overall average tuning range of ~23 nm was observed from several devices.

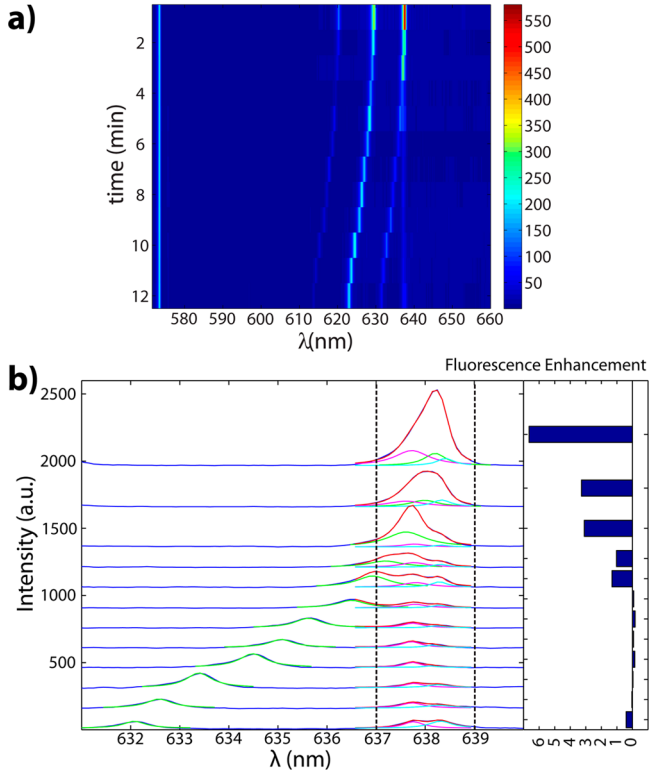

Figure 5. (a) Tuning the cavity into resonance with the ZPL of the NV center. The cavity is tuned into resonance by condensing Xe gas onto the device while continuously measuring spectra of the NV center at 4 K in a cryostat. Xe is injected into the chamber where it condenses and redshifts the resonance frequency of the cavity mode. When the cavity frequency overlaps the ZPL the fluorescence intensity is enhanced by a factor of $\chi \approx 7$. (b) Magnified and fitted version of panel a) where a split ZPL is observed. The dashed lines indicate the limits for integration when estimating the Purcell factor. The histogram at the right represents the corresponding enhancement.

while the 637 nm peak is associated with the NV center ZPL. We note that this particular NV appears to have a ZPL split into two different resonances (Figure 5b), which is attributed to strain-induced drifts in the ZPL frequency. Next, Xe gas was introduced into the cryostat through a nozzle directed at the

dx.doi.org/10.1021/nl402174g | Nano Lett. 2013, 13, 5791−5796

sample and positioned ~1 cm away from it. Spectra were then collected for different amounts of Xe introduced into the cavity and plotted in Figure 5a,b. As expected, the diamond Raman line and NV ZPL are fixed and do not move as a function of amount of introduced Xe, while the three cavity resonances red shift when the amount of Xe is increasing. We note that the cavity tuning was observed within seconds of the Xe being released after which the cavity frequencies were stable for hours, indicating no further gas dynamics. Reheating the sample to room temperature reverses the tuning. With this procedure, we were able to repeatedly tune over a range of ~7 nm in step sizes of ~0.5 nm without significant degradation of the cavity Q.

As the cavity is tuned into resonance with the ZPL of the NV center, the total signal in the ZPL band is enhanced due to the interaction with the cavity mode. This enhancement is induced by a combination of collection efficiency and Purcell enhancement for the part of the dipole fluorescence that is coupled to the cavity mode. In the case of a resonant interaction the latter is given by

$$F_P = \frac{3}{4\pi^2}\left(\frac{\lambda}{n}\right)^3 \frac{Q}{V}\frac{|\mathbf{E}_{NV}\boldsymbol{\mu}_{NV}|^2}{|\mathbf{E}_{max}|^2|\boldsymbol{\mu}_{NV}|^2} \quad (1)$$

where $E_{NV,max}$ are the cavity electric field at the position of the NV center and cavity mode maximum, respectively, μ_{NV} is the NV center dipole moment, λ is the wavelength of the cavity mode and $n = 2.4$ is the refractive index of diamond, and $V = [\int \varepsilon(\vec{r})|\vec{E}(\vec{r})|^2 d^3\vec{r}]/\max[\varepsilon(\vec{r})|\vec{E}(\vec{r})|^2]$ is the cavity mode volume.

Figure 5 shows the PLE spectrum through a series of Xe deposition steps, clearly indicating an enhancement of the ZPL intensity when the cavity comes into resonance. The spectra in Figure 5 have been normalized to the diamond Raman line at 573 nm to account for overall intensity fluctuations resulting from the Xe condensation.

By comparing the spectra when the cavity is resonant with the ZPL to those when it is off-resonant, we can obtain an estimate of the fluorescence enhancement χ. In the case of a resonant cavity (as in the top spectrum of Figure 5), the total ZPL intensity is given by

$$I_{ZPL}^{res} = (\eta_{cav}F_P + \eta_{NV})\frac{1}{\tau_0} \quad (2)$$

where $\eta_{cav,NV}$ are the overall collection efficiencies for photons emitted by the cavity and by the NV center directly, respectively, and τ_0 is the NV center excited state lifetime in the absence of any Purcell enhancement. In the off-resonant case this reduces simply to

$$I_{ZPL}^{off-res} = \frac{\eta_{NV}}{\tau_0} \quad (3)$$

Dividing eq 2 by eq 3 and further making the assumption that $\eta_{cav} = \eta_{NV}$, that is, that cavity Q is scattering-limited, we arrive at

$$\chi = \frac{\eta_{cav}F_P}{\eta_{NV}} = \frac{I_{ZPL}^{res}}{I_{ZPL}^{off-res}} - 1 \quad (4)$$

This enhancement factor χ is histogramed in the right-hand panel of Figure 5b. A maximum fluorescence enhancement of 7 is observed when the cavity is resonant with the ZPL.

This modest enhancement is substantially lower than expected given our cavity parameters. With a cavity Q of 1634 and mode volume of 3.7 $(\lambda/n)^3$, we expect an enhancement of 34 for ideal NV center placement and orientation. This discrepancy relative to our measured enhancement suggests that a substantial improvement can be gained by a more deterministic method for spatial alignment of the NV center with the cavity, in addition to improving the cavity Q factor through better fabrication.

In this work, we have described the design and fabrication of suspended, 1D photonic crystal cavities made from high-purity, single-crystal diamond and having Q factors of up to 6000. Methods for blue tuning over a range of 23 nm and red tuning over a range of 7 nm were demonstrated, culminating in the selective enhancement of the ZPL intensity of a single NV center by a factor of 7, as verified by tuning a cavity mode into resonance with the NV center's ZPL at low temperature. To facilitate the process of finding a device with a well-coupled NV center we used our lower-Q, higher mode volume design; however with our best fabricated cavities and an optimally placed NV center, we would expect an enhancement of up to 250. With smaller mode volume designs, more refined fabrication techniques to reduce side-wall roughness, and by developing deterministic methods for spatial alignment of the NV center within the cavity mode, even larger enhancement factors can be expected. Along with the recent work in 2D photonic crystals,[20] these results open up promising avenues for new technologies in quantum sensing, quantum information science, and quantum networks.[1]

The small 1D footprint and fabrication by RIE make the current approach scalable with ~1000 devices fabricated in parallel on a single chip. Additionally, the coupling to propagating waveguide modes, which occurs naturally in 1D photonic crystal devices, makes this geometry attractive for quantum networks and quantum information applications. Although improved methods must be found which allow for incorporation of these devices with implanted, stable NV centers, our method provides the framework for realizing such advanced quantum technologies.

AUTHOR INFORMATION

Corresponding Author

*E-mail: loncar@seas.harvard.edu.

Author Contributions

⊥B.J.M.H. and B.J.S. contributed equally.

Notes

The authors declare no competing financial interest.

ACKNOWLEDGMENTS

Devices were fabricated in the Center for Nanoscale Systems (CNS) at Harvard. B.H. gratefully acknowledges support from the Harvard Quantum Optics Center (HQOC). This work was supported in part by NSF, AFOSR MURI (Grant FA9550-12-1-0025), CUA and DARPA (Quiness program). M.L. acknowledges support from the Sloan Foundation.

REFERENCES

(1) Kimble, H. J. The quantum internet. *Nature* **2008**, *453*, 1023–1030.

(2) Zaitsev, A. M. *Optical Properties of Diamond: A Data Handbook*; Springer-Verlag: Berlin, 2001.

(3) Childress, L. I. *Coherent Manipulation of Single Quantum Systems in the Solid State*; The Department of Physics, Harvard University: Cambridge, MA, 2007.

(4) Wrachtrup, J.; Jelezko, F. Processing quantum information in diamond. *J. Phys.: Condens. Matter* **2006**, *18*, S807−S824.
(5) O'Brien, J. L. Optical Quantum Computing. *Science* **2007**, *318*, 1567.
(6) Neumann, P.; et al. Multipartite entanglement among single spins in diamond. *Science* **2008**, *320*, 1326.
(7) Maze, J. R.; et al. Nanoscale magnetic sensing with an individual electronic spin in diamond. *Nature* **2008**, *455*, 644−648.
(8) Balasubramanian, G.; et al. Nanoscale imaging magnetometry with diamond spins under ambient conditions. *Nature* **2008**, *455*, 648−651.
(9) Maletinsky, P.; et al. A robust scanning diamond sensor for nanoscale imaging with single nitrogen-vacancy centres. *Nat. Nanotechnol.* **2012**, *7*, 320.
(10) Childress, L.; Taylor, J. M.; Sorensen, A. S.; Lukin, M. D. Fault-tolerant quantum communication based on solid-state photon emitters. *Phys. Rev. Lett.* **2006**, *96*, 070504.
(11) Beveratos, A.; et al. Single photon quantum cryptography. *Phys. Rev. Lett.* **2002**, *89*, 187901.
(12) Reithmaier, J. P.; et al. Strong coupling in a single quantum dot−semiconductor microcavity system. *Nature* **2004**, *432*, 197.
(13) Yoshie, T.; et al. Vacuum Rabi splitting with a single quantum dot in a photonic crystal nanocavity. *Nature* **2004**, *432*, 200.
(14) Englund, D.; et al. Deterministic Coupling of a Single Nitrogen Vacancy Center to a Photonic Crystal Cavity. *Nano Lett.* **2010**, *10*, 3922−3926.
(15) Wolters, J.; et al. Enhancement of the zero phonon line emission from a single nitrogen vacancy center in a nanodiamond via coupling to a photonic crystal cavity. *Appl. Phys. Lett.* **2010**, *97*, 141108.
(16) van der Sar, T.; et al. Deterministic nanoassembly of a coupled quantum emitter−photonic crystal cavity system. *Appl. Phys. Lett.* **2011**, *98*, 193103.
(17) de Leon, N. P.; et al. Tailoring Light-Matter Interaction with a Nanoscale Plasmon Resonator. *Phys. Rev. Lett.* **2012**, *108*, 226803.
(18) Faraon, A.; Barclay, P. E.; Santori, C.; Fu, K.-M. C.; Beausoleil, R. G. Resonant enhancement of the zero-phonon emission from a colour centre in a diamond cavity. *Nat. Photonics* **2011**, *5*, 301.
(19) Hausmann, B. M.; et al. Integrated Diamond Networks for Quantum Nanophotonics. *Nano Lett.* **2012**, *12*, 1578.
(20) Faraon, A.; Santori, C.; Huang, Z.; Acosta, V. M.; Beausoleil, R. G. Coupling of Nitrogen-Vacancy Centers to Photonic Crystal Cavities in Monocrystalline Diamond. *Phys. Rev. Lett.* **2012**, *109*, 033604.
(21) Riedrich-Moeller, J. et al. One- and two-dimensional photonic crystal microcavities in single crystal diamond. *Nat. Nanotechnol. 7* (**2012**).
(22) Burek, M. J.; et al. Free-Standing Mechanical and Photonic Nanostructures in Single-Crystal Diamond. *Nano Lett.* **2012**, *12*, 6084.
(23) Ahn, B. H.; et al. One-dimensional parabolicbeam photonic crystal laser. *Opt. Exp.* **2010**, *18*, 5654−5660.
(24) Quan, Q.; Loncar, M. Deterministic design of wavelength scale, ultra-high Q photonic crystal nanobeam cavities. *Opt. Exp.* **2011**, *19*, 18529−18542.
(25) Quan, Q.; Deotare, P. B.; Loncar, M. Photonic crystal nanobeam cavity strongly coupled to the feeding waveguide. *Appl. Phys. Lett.* **2010**, *96*, 203102.
(26) Kimble, H. J.; Dagenais, M.; Mandel, L. Photon Antibunching in Resonance Fluorescence. *Phys. Rev. Lett.* **1977**, *39*, 691.
(27) Mosor, S.; et al. Scanning a photonic crystal slab nanocavity by condensation of xenon. *Appl. Phys. Lett.* **2005**, *87*, 141105.